

Langevin Model of the Temperature and Hydration Dependence of Protein Vibrational Dynamics

Kei Moritsugu^{†,‡} and Jeremy C. Smith^{*,†}

[†]Computational Molecular Biophysics, Interdisciplinary Center for Scientific Computing (IWR), University of Heidelberg, Im Neuenheimer Feld 368, 69120 Heidelberg, Germany, and [‡]Graduate School of Material Science, Nara Institute of Science and Technology (NAIST), 630-0192 Nara, Japan

Received: December 16, 2004; In Final Form: April 8, 2005

The modification of internal vibrational modes in a protein due to intraprotein anharmonicity and solvation effects is determined by performing molecular dynamics (MD) simulations of myoglobin, analyzing them using a Langevin model of the vibrational dynamics and comparing the Langevin results to a harmonic, normal mode model of the protein in vacuum. The diagonal and off-diagonal Langevin friction matrix elements, which model the roughness of the vibrational potential energy surfaces, are determined together with the vibrational potentials of mean force from the MD trajectories at 120 K and 300 K in vacuum and in solution. The frictional properties are found to be describable using simple phenomenological functions of the mode frequency, the accessible surface area, and the intraprotein interaction (the displacement vector overlap of any given mode with the other modes in the protein). The frictional damping of a vibrational mode in vacuum is found to be directly proportional to the intraprotein interaction of the mode, whereas in solution, the friction is proportional to the accessible surface area of the mode. In vacuum, the MD frequencies are lower than those of the normal modes, indicating intramolecular anharmonic broadening of the associated potential energy surfaces. Solvation has the opposite effect, increasing the large-amplitude vibrational frequencies relative to in vacuum and thus vibrationally confining the protein atoms. Frictional damping of the low-frequency modes is highly frequency dependent. In contrast to the damping effect of the solvent, the vibrational frequency increase due to solvation is relatively temperature independent, indicating that it is primarily a structural effect. The MD-derived vibrational dynamic structure factor and density of states are well reproduced by a model in which the Langevin friction and potential of mean force parameters are applied to the harmonic normal modes.

1. Introduction

Protein function is mediated by anharmonic internal dynamics on a rugged potential energy surface.^{1,2} Anharmonic motions can be examined using molecular dynamics (MD) simulation.³ However, MD results in a large numbers of time-dependent positions that are sometimes difficult to interpret unambiguously. To simplify the results of MD simulations, principal component analysis (PCA) has been widely used, in which the variance–covariance matrix of the interatomic fluctuations is diagonalized, leading to a quasiharmonic approximation of the positional fluctuations as a set of uncorrelated harmonic distribution functions.^{4–8} The anharmonicity can then be analyzed via the nonquadratic parts of the equilibrium distributions.

PCA is a potential of mean force (PMF) approach, providing effective collective coordinates and their corresponding free energies. To complement PCA, it is necessary to derive a description of the associated dynamics. One method for doing this is Langevin mode analysis, in which a frictional and a stochastic force are introduced into the equation of motion.^{9–15} These additional terms make possible the determination of dynamical perturbations arising from temperature, solvent

effects, and the anharmonic coupling between protein vibrations. The dynamical perturbations are treated via the friction matrix. In the present study, we focus on the modeling and physical interpretation of the friction matrix for protein dynamics within the framework of the Langevin model.

In one previous study, frictional effects were estimated by fitting a model to experimental neutron scattering spectra in which each protein normal mode is considered as an independent damped Langevin oscillator.¹⁶ In an alternative study, friction effects were calculated with models combining normal-mode analysis with hydrodynamic theory.^{9,10,13} The simplest thermodynamic model is Stokes' law, in which the diagonal friction is derived using the linear Navier–Stokes equation.¹⁷ With this model, the friction on each atom is calculated via the force exerted on a sphere of a given hydrodynamic radius moving at a constant velocity in a fluid of constant viscosity. The hydrodynamic radii have been estimated using a function of the solvent-accessible surface area (ASA).¹⁸ However, the Stokes model oversimplifies the solvent contribution¹⁹ and also neglects intraprotein anharmonicity.

An appropriate procedure for overcoming the above difficulties is direct calculation of the friction matrix from MD simulation, which explicitly includes the full intramolecular and solvent interactions.^{11,12,14,15,20} Here, we employ this approach to determine the Langevin friction matrix for myoglobin. Comparisons are made of the friction matrixes derived from

* Author to whom correspondence should be addressed. E-mail: biocomputing@iwr.uni-heidelberg.de. Telephone: +49-6221-54-8857. Fax: +49-6221-54-8868.

[†] University of Heidelberg.

[‡] Nara Institute of Science and Technology (NAIST).

MD trajectories in vacuum and in water and at 120 K (below the dynamical “glass” transition temperature of $T_g \sim 180\text{--}220$ K^{21–23}) and at 300 K (room temperature). This comparison allows a physical interpretation of the friction by decomposition into contributions from solvation and from intraprotein interaction. Temperature- and solvent-induced frequency shifts in the harmonic potential of mean force of protein vibrations are also determined. On the basis of the results obtained, physically intuitive model functions are derived for the friction matrix elements and of the PMF for the complex anharmonic dynamics of myoglobin. The emphasis in the present article is on vibrational dynamics in the protein. Thus, the questions addressed concern the modification of the effective vibrational frequencies with temperature and hydration and the associated frictional effects.

We also examine here the validity of the Langevin model by calculating inelastic neutron scattering spectra, which are directly determined by the picosecond time scale atomic dynamics. It is shown that the Langevin model with the friction matrix and harmonic PMF derived by model functions can reproduce the vibrational aspects of the inelastic neutron scattering spectra. Finally, a physical model of internal protein dynamics is proposed that combines the potential energy surface with the Langevin model friction, i.e., both the harmonic potential of mean force and the frictional contribution.

2. Theory and Methods

2.1. Dynamical Simulations. In the present study, the simulation data to which the Langevin model was fitted were derived using molecular dynamics simulations and normal-mode analyses of carboxymyoglobin (the Protein Data Bank structure: 1A6G²⁴). The CHARMM program version 30b2²⁵ was used to perform the simulations with the CHARMM all-atom parameter set 22²⁶ for the potential function.

The MD simulations of myoglobin were carried out at 120 K and at 300 K in two different environments: in vacuum and in water. All four MD simulations were performed for 1 ns with an integration time step of 0.5 fs. Both the atomic coordinates and velocities were saved every 5 fs for analysis.

The vacuum simulations were performed in the microcanonical ensemble with the average kinetic energy corresponding to the system temperature. All pairwise electrostatic interactions were included, i.e., without truncation. The dielectric constant was taken as distance-dependent ($\epsilon = r$). For the simulation in aqueous solvents, a rectangular box was constructed of dimensions $56 \text{ \AA} \times 52 \text{ \AA} \times 41 \text{ \AA}$ and fully solvated with 3090 TIP3 water molecules.²⁷ One chloride ion was placed in the box so as to neutralize the net protein charge. The simulation in water was performed under constant temperature and constant pressure (1 atm) conditions (the NPT ensemble). The temperature and pressure were controlled using the Nosé–Hoover algorithm^{28,29} with mass parameters of $Q_T = 2000$ amu and $Q_P = 2500$ amu, respectively. Periodic boundary conditions were imposed on the box. Electrostatic interactions were calculated using the particle-mesh Ewald method^{30,31} with a dielectric constant of 1. The real space summation was truncated at 12 \AA using $\kappa = 0.23 \text{ \AA}^{-1}$. The configurations of the water molecules were constrained using the SHAKE algorithm.³²

The vacuum and solution simulations differ in the force field used and in the simulation procedure. In the vacuum simulation, the dielectric constant ϵ was set to $\epsilon = r$, whereas in solution, $\epsilon = 1$. The reason for this choice is to prevent the artificial, unstable conditions in the vacuum MD which have, in the past, been commonly experienced using $\epsilon = 1$. Although $\epsilon = r$ does

qualitatively mimic solvent dielectric screening, frictional properties are not modeled in this way.¹⁹ However, to examine the effect of this choice of ϵ , an additional vacuum simulation was performed at 300 K with $\epsilon = 1$. No significant effect was seen on the frictional properties examined (results not shown). Moreover, the root-mean-square (RMS) fluctuations in both simulations are similar (0.68 \AA for $\epsilon = 1$ and 0.70 \AA for $\epsilon = r$).

The second difference lies in the statistical mechanical ensemble used. For the vacuum calculation, this was microcanonical, whereas for the solution simulation, it was NPT. The reason for this choice is that NPT is impractical for vacuum simulations but is most widely used for reproducing liquid-state properties. Again, to check for any possible effect on the present results, a microcanonical solution MD simulation at 300 K was also performed. The RMS fluctuations were also similar (0.65 \AA for the microcanonical ensemble and 0.64 \AA for the NPT ensemble), and again, variation of the statistical mechanical ensemble was found to have little effect on the Langevin properties, i.e., the vibrational frequency and damping coefficients of the velocity-autocorrelation functions (results not shown). This is probably due to the equilibrium condition, i.e., fluctuations of kinetic energy and internal pressure occur evenly around the set temperature and pressure.

Normal-mode analyses were performed at 120 and 300 K with the vacuum model and potential function. For these, the average coordinates of the 1-ns MD vacuum trajectories were used as the starting structure. The structures were energy minimized with 1000 steps of the steepest descent method, followed by adopted basis Newton–Raphson minimization until a RMS energy gradient was reached of $<10^{-5} \text{ kcal/mol/\AA}$ (~ 3000 steps at 120 K and ~ 6400 steps at 300 K). The mass-weighted second-derivative matrixes calculated using the minimized structures were diagonalized to yield the normal-mode eigenvectors and eigenvalues.

2.2. Langevin Mode Analysis. A quasiharmonic method of analysis of protein dynamics has been developed on the basis of the Langevin equation.^{9–15} The analysis simplifies the behavior of the system by describing it as a linear combination of underdamped and overdamped motions called “Langevin modes”. In the Langevin model, the complex potential energy surface is approximated by a harmonic potential of mean force, and the damping due to the surrounding solvent and to the intraprotein interaction is included via the friction matrix.

The Langevin equation is

$$m_i \frac{d^2}{dt^2} q_i + \frac{\partial V(\mathbf{q})}{\partial q_i} + \sum_j \zeta_{ij} \dot{q}_j = R_i(t) \quad (1)$$

where q_i is the coordinate of atom i ($i = 1, \dots, N$, where N is the number of atoms), m_i is the mass, and $-\partial V(\mathbf{q})/\partial q_i \equiv f_i$, is the force exerted on the atom. The friction matrix elements are ζ_{ij} . $R_i(t)$ is a random force satisfying the conditions

$$\langle R_i(t) \rangle = 0 \quad (2)$$

$$\langle R_i(0) R_j(t) \rangle = 2\beta^{-1} \zeta_{ij} \delta(t)$$

where $\langle \rangle$ denotes an ensemble average and $\delta(t)$ is the delta function. $\beta = 1/k_B T$ where T is the temperature and k_B is the Boltzmann constant.

Assuming that the potential energy is harmonic around the equilibrium position, $\mathbf{q}^0 = \{q_i^0\}$, i.e.,

$$V(\mathbf{q}) \approx V(\mathbf{q}^0) + \frac{1}{2} \sum_{ij} \frac{\partial^2 V}{\partial q_i \partial q_j} (q_i - q_i^0)(q_j - q_j^0) \quad (3)$$

then the equations of motion in matrix format are as follows,

$$\dot{\alpha} = \mathbf{B}\alpha + \begin{pmatrix} 0 \\ \mathbf{R}(t) \end{pmatrix} \quad (4)$$

where

$$\alpha = \begin{pmatrix} \mathbf{x} \\ \mathbf{v} \end{pmatrix}, \quad \mathbf{B} = \begin{pmatrix} 0 & 1 \\ -\mathbf{F} & -\gamma \end{pmatrix}$$

$$x_i = m_i^{1/2}(q_i - q_i^0) \quad F_{ij} = \frac{\partial^2 V}{\partial q_i \partial q_j} m_i^{-1/2} m_j^{-1/2} \quad (5)$$

$$v_i = m_i^{1/2} \dot{q}_i \quad \gamma_{ij} = \zeta_{ij} m_i^{-1/2} m_j^{-1/2}$$

From the solution of eq 4, a matrix of time-correlation functions is derived as,

$$\mathbf{C}(t) \equiv \langle \alpha(t) \alpha^T(0) \rangle = \beta^{-1} e^{\mathbf{B}t} \begin{pmatrix} \mathbf{F}^{-1} & 0 \\ 0 & 1 \end{pmatrix} \quad (6)$$

In terms of the eigenvalues, λ_n , and eigenvectors, \mathbf{u}_n , of the nonsymmetric matrix \mathbf{B} (i.e., $\mathbf{B}\mathbf{u}_n = \mathbf{u}_n \lambda_n$), $\exp(\mathbf{B}t)$ can be solved as $\mathbf{U}e^{\Delta t}\mathbf{U}^{-1}$, where $\mathbf{U} = (\mathbf{u}_1, \mathbf{u}_2, \dots)$, $\Delta = (\lambda_n \delta_{nm})$, and δ_{nm} is the Kronecker delta. Each eigenvalue consists of a negative real part, $-\gamma_n/2$, and an imaginary part, ω_n , i.e., $\lambda_n = -\gamma_n/2 + i\omega_n$. If ω_n is not zero, the mode exhibits oscillatory damping, whereas if ω_n is zero, the mode is overdamped. Thus the time-correlation function $\mathbf{C}(t)$ can be expressed as a linear combination of underdamped and overdamped oscillators.⁹

Langevin mode analysis requires as parameters the second-derivative matrix, \mathbf{F} , and the friction matrix, γ . These parameters are related to the time-correlation functions of phase space in eq 6 as follows.^{11,12}

$$\mathbf{F}_{ij}^{-1} = \beta \langle x_i(0) x_j(0) \rangle$$

$$\gamma_{ij} = -\beta \frac{d}{dt} \langle v_i(t) v_j(0) \rangle|_{t=0} \quad (7)$$

2.3. Calculation of Friction Matrix. The friction matrix originates from damping by both surrounding solvent molecules and intraprotein interaction. In the present study, we concentrate on the frequency dependence of the friction. For this purpose, the friction matrix was calculated on the basis of normal modes. The normal-mode friction matrix, γ_{mode} , is related to the Cartesian friction matrix, γ_{atom} , as follows.

$$\gamma_{\text{mode}} = \mathbf{U}^T \gamma_{\text{atom}} \mathbf{U} \quad (8)$$

The matrix, \mathbf{U} , is derived using normal-mode analysis (NMA), i.e., the eigenvalue problem of $\mathbf{F}\mathbf{U} = \mathbf{U}\Delta$, where $\Delta = (\Delta_{nm}) = (\omega_n^2 \delta_{nm})$ is the eigenvalue matrix and ω_n is the frequency of each mode.

The friction matrix was obtained directly on the normal-mode basis (without calculation of the Cartesian friction followed by its transformation in eq 8), i.e., by calculating the velocity-autocorrelation function (VACF) of normal modes from the MD trajectories and then γ_{nm} , i.e., the friction matrix element between normal mode n and m , from eq 7. In contrast to the harmonic potential energy surface approximated by NMA, MD

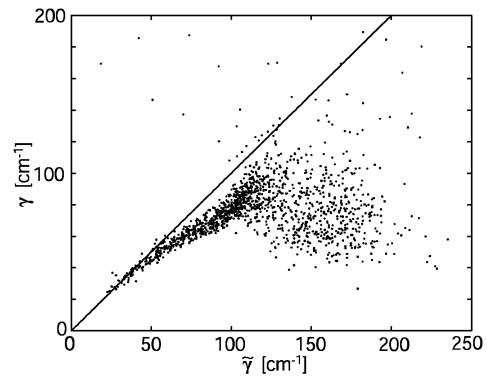


Figure 1. Diagonal friction, γ , in water at 300 K, calculated by fitting the MD-derived velocity-autocorrelation function to eq 9, is plotted against the friction calculated by linear regression over 5–25 fs, $\bar{\gamma}$.

simulation is performed on the full anharmonic potential energy surface. For a protein in vacuum, intraprotein anharmonicity determines the friction matrix. Subsequent comparison of the results derived from MD simulation in vacuum with those in water allows the perturbation due to the solvent effects to be determined.

Precise numerical calculation of the time derivative in eq 7 is essential for obtaining an accurate friction matrix. Simple linear regression in the vicinity of $t = 0$ results in errors due to vibrational dephasing, especially in the higher-frequency modes.¹¹ To overcome this difficulty, the velocity-autocorrelation function derived from the one-dimensional Langevin model¹² was directly applied as a fitting function, i.e.,

$$\psi_n(t) = \frac{\langle v_n(0) v_n(t) \rangle}{\langle v_n^2 \rangle} = \begin{cases} e^{(-\gamma_{nn}t/2)} \left(\cos \omega_n t - \frac{\gamma_{nn}}{2\omega_n} \sin \omega_n t \right) & \gamma_{nn} < 2\omega_n \\ \frac{-\gamma_{nn}/2 + \omega_{0,n}}{2\omega_{0,n}} e^{(-\gamma_{nn}/2 + \omega_{0,n})t} + \frac{\gamma_{nn}/2 + \omega_{0,n}}{2\omega_{0,n}} e^{(-\gamma_{nn}/2 - \omega_{0,n})t} & \gamma_{nn} \geq 2\omega_n \end{cases} \quad (9)$$

where $\omega_n = \sqrt{\omega_n^2 - \gamma_{nn}^2/4}$ is the effective frequency for underdamped modes ($\gamma_{nn} < 2\omega_n$) and $\omega_{0,n} = \sqrt{\gamma_{nn}^2/4 - \omega_n^2}$ holds for overdamped modes ($\gamma_{nn} \geq 2\omega_n$). The time derivative at $t = 0$ of eq 9 is γ_{nn} , which is in agreement with eq 7, using the relation, $\langle v_n^2 \rangle = 1/\beta$. Equation 9 allows fitting over a much longer time scale than that of simple linear regression, thus allowing the contribution to the decay of the velocity-autocorrelation function from the friction to be separated from the vibrational dephasing. Both of the two model functions in eq 9 were fitted to the simulation-derived velocity-autocorrelation function over the range of $t = 0$ –5 ps. Then, the integral of square deviation between the MD and model VACF, i.e., $\int_0^5 dt |\psi_{\text{MD}}(t) - \psi_{\text{model}}(t)|^2$, was calculated for the two models as an evaluation function, allowing determination of whether the associated dynamics is underdamped or overdamped.

In Figure 1 the diagonal friction obtained by linear regression (5–25 fs) is compared with that obtained by fitting to the model function (eq 9). The linear regression overestimates the frictions, especially in the higher-frequency region $> \sim 100 \text{ cm}^{-1}$, because of the contribution of vibrational dephasing. In what follows, the direct fitting of the MD-derived velocity-autocorrelation

function to the model functions in eq 9 was used for calculating the diagonal friction.

In contrast to the diagonal friction, no appropriate fitting function (such as eq 9) is available for calculating the off-diagonal friction via eq 7. Thus, the off-diagonal friction elements were calculated from the gradient of the velocity cross-correlation function in eq 7 using linear regression over the range of $t = 5\text{--}25$ fs. The procedure leads to numerical errors in the higher frequency modes $\omega > \sim 100\text{ cm}^{-1}$, as illustrated in Figure 1. Consequently, only those matrix elements, γ_{nm} , with frequencies, $\omega_n, \omega_m < 100\text{ cm}^{-1}$, were considered.

2.4. Dynamic Structure Factor. The dynamics of a protein molecule can be described by the time evolution of the spatial correlation of each atom. The space- and time-dependent distribution function, $G(\mathbf{r}, t)$, introduced by van Hove,³³ is given as follows:

$$G(\mathbf{r}, t) = \frac{1}{N} \left\langle \sum_{i=1}^N \sum_{j=1}^N \delta[\mathbf{r} + \mathbf{r}_j(0) - \mathbf{r}_i(t)] \right\rangle \quad (10)$$

The physical interpretation of the van Hove correlation function is that $G(\mathbf{r}, t)$ is proportional to the probability of finding a particle i at a point \mathbf{r} at time t , given that there was a particle j at the origin $\mathbf{r} = \mathbf{0}$ at time $t = 0$. The function G can be separated into two terms, usually called the “self” and “distinct” parts.

$$G(\mathbf{r}, t) = G_s(\mathbf{r}, t) + G_d(\mathbf{r}, t) \quad (11)$$

where

$$G_s(\mathbf{r}, t) = \frac{1}{N} \left\langle \sum_{i=1}^N \int \delta[\mathbf{r} + \mathbf{r}_i(0) - \mathbf{r}_i(t)] \right\rangle \quad (12)$$

$$G_d(\mathbf{r}, t) = \frac{1}{N} \left\langle \sum_{i=1}^N \sum_{j \neq i}^N \int \delta[\mathbf{r} + \mathbf{r}_j(0) - \mathbf{r}_i(t)] \right\rangle \quad (13)$$

The incoherent intermediate scattering function, $F_s(\mathbf{q}, t)$, and its time Fourier transform, the incoherent dynamic structure factor, $S_s(\mathbf{q}, \omega)$, are defined in terms of the self part of the van Hove correlation function as follows,

$$F_s(\mathbf{q}, t) = \int d\mathbf{r} G_s(\mathbf{r}, t) e^{-i\mathbf{q} \cdot \mathbf{r}} = \sum_{i=1}^N \langle e^{-i\mathbf{q} \cdot \mathbf{r}_i(0)} e^{-i\mathbf{q} \cdot \mathbf{r}_i(t)} \rangle \quad (14)$$

$$S_s(\mathbf{q}, \omega) = \frac{1}{2\pi} \int F_s(\mathbf{q}, t) e^{-i\omega t} dt \quad (15)$$

The incoherent neutron scattering cross section is related to $S_s(\mathbf{q}, \omega)$ by weighting the time-correlation function of atom i in eq 14 by the square of the isotopic incoherent scattering length, $b_{\text{inc}, i}^2$, i.e.,

$$\left[\frac{\delta^2 \sigma_{\text{inc}}}{\delta \Omega \delta \omega} \right]_{\text{vib}} = \frac{k_f}{k_i} S(\mathbf{q}, \omega) \quad (16)$$

where

$$S(\mathbf{q}, \omega) = \frac{1}{2\pi} \int F(\mathbf{q}, t) e^{-i\omega t} dt \quad (17)$$

$$F(\mathbf{q}, t) = \sum_{i=1}^N b_{\text{inc}, i}^2 \langle e^{-i\mathbf{q} \cdot \mathbf{r}_i(0)} e^{i\mathbf{q} \cdot \mathbf{r}_i(t)} \rangle \quad (18)$$

The left side of eq 16 is the incoherent scattering in a differential solid angle $\delta\Omega$ with an energy bandwidth, $\delta\omega$, at a given neutron energy transfer, $\hbar\omega$. The momentum transfer is $\hbar\mathbf{q} = \hbar\mathbf{k}_f - \hbar\mathbf{k}_i$, where \mathbf{k}_i and \mathbf{k}_f are the incident and final neutron scattering vectors, respectively.

Here, the dynamic structure factor was evaluated numerically from molecular dynamics trajectories using eqs 17 and 18.^{34–36} In these calculations, $|\mathbf{q}|$ was set to 2 \AA^{-1} and averaged over three orthogonal directions. The energy resolution function was assumed to be a Gaussian with variance, $\Delta E = 30\text{ }\mu\text{eV}$, which corresponds to typical experimental instrumental energy resolutions.³⁷ For the spectra calculated from the MD simulations, 2^{16} trajectory frames separated by 10 fs (total length of ~ 640 ps) were used.

$S(\mathbf{q}, \omega)$ can also be evaluated by assuming a dynamical model, allowing an analytical derivation of $F(\mathbf{q}, t)$. Using the Langevin model discussed in Section 2.1 and assuming that the friction matrix is diagonal ($\gamma_{nm} = \gamma_n \delta_{nm}$), $F(\mathbf{q}, t)$ is derived in the classical form as,^{12,17,38}

$$F(\mathbf{q}, t) = \sum_{i=1}^N b_{\text{inc}, i}^2 \exp \left\{ -q^2 \sum_{n=1}^{3N-6} \frac{k_B T}{m_i \omega_n^2} \left| \mathbf{q} \cdot \mathbf{u}_n^{(i)} \right|^2 [1 - \varphi_n(t)] \right\} \quad (19)$$

where

$$\varphi_n(t) \equiv \frac{\langle x_n(0)x_n(t) \rangle}{\langle x_n^2 \rangle} = \begin{cases} e^{-\gamma_{nn}t/2} \left(\cos \bar{\omega}_n t + \frac{\gamma_{nn}}{2\bar{\omega}_n} \sin \bar{\omega}_n t \right) & \gamma_{nn} < 2\bar{\omega}_n \\ \frac{\gamma_{nn}/2 + \bar{\omega}_{0,n}}{2\bar{\omega}_{0,n}} e^{(-\gamma_{nn}/2 + \bar{\omega}_{0,n})t} + \frac{-\gamma_{nn}/2 + \bar{\omega}_{0,n}}{2\bar{\omega}_{0,n}} e^{(-\gamma_{nn}/2 - \bar{\omega}_{0,n})t} & \gamma_{nn} \geq 2\bar{\omega}_n \end{cases} \quad (20)$$

ω_n and γ_{nn} are the frequency and the friction coefficient of mode n , respectively, and $\mathbf{u}_n^{(i)}$ is the displacement of atom i in the eigenvector \mathbf{u}_n .

To examine the usefulness of the Langevin model, a comparison was made of $S(\mathbf{q}, \omega)$ derived from the intermediate scattering function calculated using the Langevin model in eq 19, with both the frequency, ω_n , and friction, γ_n , derived from the MD simulation and with $S(\mathbf{q}, \omega)$ derived directly from the MD simulation using eq 17. To permit this comparison with the spectra from the classical MD, classical-mechanical scattering function was used. Therefore, the comparison is only applicable to the low-frequency region, in which quantum mechanical effects can be neglected ($\hbar\omega \ll k_B T$).¹⁶

2.5. Vibrational Density of States. The vibrational density of states, $g(\omega)$, i.e., the vibrational frequency distribution, was calculated from the MD trajectory as the Fourier transform of the velocity-autocorrelation function, i.e.,

$$g(\omega) = \sum_{i=1}^N \frac{1}{2\pi} \int_{-\infty}^{\infty} \langle \mathbf{v}_i(0) \cdot \mathbf{v}_i(t) \rangle / \langle \mathbf{v}_i^2 \rangle e^{-i\omega t} dt \quad (21)$$

From the Langevin model with the friction, γ_{nn} , and the frequency, ω_n , of mode n , $g(\omega)$ is given as^{11,12}

$$g(\omega) = \sum_{n=1}^{3N-6} \frac{1}{\pi} \frac{\gamma_{nn}\omega^2}{(\omega^2 - \omega_n^2)^2 + \gamma_{nn}^2\omega^2} \quad (22)$$

The vibrational density of states is related to the dynamic structure factor in the classical limit as

$$g(\omega) = \lim_{q \rightarrow 0} \frac{\omega^2}{q^2} S_s(\mathbf{q}, \omega) \quad (23)$$

Therefore, $g(\omega)$ can also be derived from neutron scattering experiments.³⁹

In a manner similar to $S(\mathbf{q}, \omega)$, $g(\omega)$ calculated directly from the MD simulation was compared with the Langevin vibrational density of states. For the spectra calculated from the MD simulations, 2¹⁶ trajectory frames separated by 10 fs (total length of ~640 ps) were used.

3. Results and Discussion

In this section, the friction matrix and the vibrational potential of mean force, calculated assuming the Langevin model in eq 1 for the dynamics of myoglobin, are presented. The Langevin parameters are analyzed by decomposing them into contributions from intraprotein interaction and from solvation, depending on temperature. Model functions are constructed with, as variables, the frequency and properties originating from the displacement vectors of normal modes. Finally, the validity of the Langevin model is examined by comparing the dynamic structure factor and the vibrational density of states calculated from the model with those derived directly from the MD simulations.

3.1. Friction Matrix and Potential of Mean Force. The friction matrixes and the harmonic potentials of mean force were calculated from MD simulations in both vacuum and water, and at both 120 and 300 K. The diagonal parts (corresponding to the autocorrelation of each mode) and the off-diagonal parts (corresponding to coupling between pairs of modes) of the friction matrix are now separately analyzed. To focus on the friction exerted on the collective motions, only those matrix elements are examined that correspond to modes of $\omega < 300 \text{ cm}^{-1}$. The intraprotein interaction with the higher-frequency vibrations ($> 300 \text{ cm}^{-1}$) is thus considered to be projected into the random force of the Langevin model in eq 1.

3.1.1. Diagonal Friction and Potential of Mean Force. In contrast to the simplified, normal-mode model, the MD trajectories include the complex anharmonic dynamics on the full, rugged potential surface. In the Langevin model the friction originates from the random force through the roughness of this potential energy surface. The friction calculated from MD in a vacuum thus originates from the roughness of the intraprotein surface, and the temperature dependence of this friction arises from changes in the intraprotein potential energy surface. Comparing the vacuum MD friction with that in water allows the contribution of solvation to the friction matrix to be estimated.

The diagonal friction and the frequency of the harmonic potential of mean force were calculated as a function of the NMA frequency, $\omega = \omega_{\text{NMA}}$, by fitting the MD-derived velocity correlation function of each normal mode to eq 9 using the MD trajectories in vacuum (γ_{vacuum} and ω_{vacuum}) and in water (γ_{water} and ω_{water}). The diagonal friction is shown in Figure 2a. No overdamped modes were found at 120 K in vacuum and in water nor at 300 K in vacuum. In contrast, 11 modes, all with $\omega_{\text{NMA}} < 13 \text{ cm}^{-1}$, are overdamped at 300 K in water (shown in the inset of Figure 2a4).

To examine the relationship between γ_{nn} (the suffix nn is dropped in the following discussion as well as the suffix n of ω_n) and the normal-mode displacement vector, \mathbf{u}_n , the normal-mode information entropy was calculated as the “localization factor”, L_n , defined as follows:⁴⁰

$$L_n = - \sum_i |\mathbf{u}_n^{(i)}|^2 \log |\mathbf{u}_n^{(i)}|^2 \quad (24)$$

where $\mathbf{u}_n^{(i)}$ is the mass-weighted displacement of atom i in the eigenvector of mode n . $|\mathbf{u}_n^{(i)}|^2 = p_n(i)$ is the proportion that atom i makes to the displacement vector of mode n (i.e., $\sum_i p_n(i) = 1$). Thus, $\exp(L_n)$ can be estimated as the number of atoms active in mode n . L_n versus ω , plotted in Figure 3a, shows that the low-frequency modes are more collective and that the motion becomes more local with increasing mode frequency.

The distribution of friction coefficients, γ , in Figure 2a is broad, the distribution width, $\Delta\gamma$, being $\sim 20 \text{ cm}^{-1}$ for $\omega < 100 \text{ cm}^{-1}$ (denoted here as “low-frequency modes”). For $\omega > 100 \text{ cm}^{-1}$ (denoted here as “high-frequency modes”), the distribution is even more spread out ($\Delta\gamma$ is nearly equal to the average of γ). Test calculations showed that the spread of γ distribution is not due to lack of sampling in the MD trajectories. Rather, the variation of γ for modes close together in frequency arises from differences in the atomic displacement vectors of the normal modes. Whereas the low-frequency modes are collective, with the consequence that friction-determining characteristics such as solvent interactions are roughly similar among these modes, the high-frequency modes are more local, resulting in large differences in the friction-determining characteristics and thus a wide $\Delta\gamma$.

Two further quantities are potentially useful in characterizing the frictional property of a normal-mode displacement vector. One is the “intraprotein interaction” of a pair of modes, n, m .

$$S_{nm} = \sum_i |\mathbf{u}_n^{(i)} \cdot \mathbf{u}_m^{(i)}| \quad (25)$$

The overall intraprotein interaction of mode n , i.e., the interaction with all the other modes, is the average of the pairwise contributions:

$$S_n = \frac{1}{3N-7} \sum_{m \neq n}^{3N-6} S_{nm} \quad (26)$$

In Figure 3b S_n is plotted against the normal-mode frequency. The collective, low-frequency modes ($< 100 \text{ cm}^{-1}$) have similar magnitudes of S_n , whereas the higher-frequency modes have a broad distribution as wide as the average (i.e., $\Delta S/S \approx 1$).

The second quantity is the average amplitude-weighted water-accessible surface area of a mode, A_n , defined as follows,

$$A_n = \sum_i |\mathbf{u}_n^{(i)}|^2 \sigma_i \quad (27)$$

where σ_i is the accessible surface area of atom i . Figure 3c shows that the very low-frequency modes ($< 50 \text{ cm}^{-1}$) have relatively high A_n values, whereas the higher-frequency modes have a wide spread of A_n . This depends on whether the local vibration occurs at the surface or in the interior of the protein. S_n and A_n will be subsequently used in deriving model functions for the frequency-dependent friction.

Figure 2a also reveals the effects of temperature and solvation on the friction. At 300 K, the friction is larger than at 120 K because of increased sampling of the anharmonic region of the

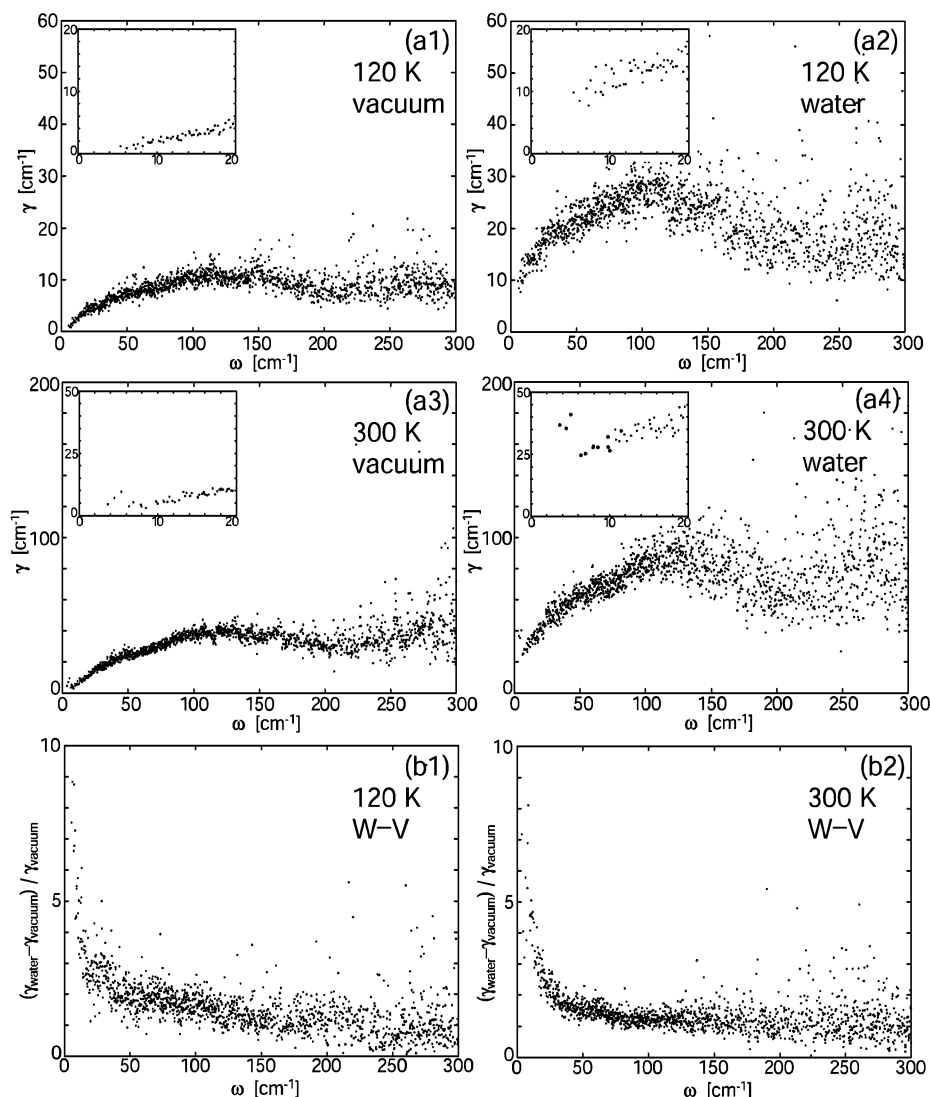


Figure 2. (a) Diagonal friction as a function of normal-mode frequency, $\gamma(\omega)$, derived from MD simulation (1) in vacuum at 120 K, (2) in water at 120 K, (3) in vacuum at 300 K, and (4) in water at 300 K. The results for frequencies < 20 cm⁻¹ are plotted in the insets on an enlarged scale. Overdamped modes are visible in the inset of (a4) as enlarged dots. (b) Relative friction increase, $(\gamma_{\text{water}} - \gamma_{\text{vacuum}}) / \gamma_{\text{vacuum}}$, calculated from MD in water and in vacuum, plotted against normal-mode frequency. (1) MD at 120 K and (2) MD at 300 K.

potential energy surface. The effect of solvation can be quantified by the relative friction increase, i.e., $(\gamma_{\text{water}} - \gamma_{\text{vacuum}}) / \gamma_{\text{vacuum}}$, shown in Figure 2b. The friction increase via solvation, $\gamma_{\text{water}} - \gamma_{\text{vacuum}}$, is larger at 300 K because γ_{vacuum} is larger at 300 K than at 120 K and $(\gamma_{\text{water}} - \gamma_{\text{vacuum}}) / \gamma_{\text{vacuum}}$ is nearly the same at both temperatures. This indicates that the solvent effect on the friction is determined by the dynamic fluctuation of the water molecules. The modes lower than 100 cm⁻¹ exhibit large solvation effects, i.e., $(\gamma_{\text{water}} - \gamma_{\text{vacuum}}) / \gamma_{\text{vacuum}} > 1$. This ratio becomes closer to 0 with increasing mode frequency. The collective low-frequency modes (with large L_n in eq 24) are strongly modified by solvent because of their large accessible surface areas (A_n in eq 27).

Comparison can be made of the above results with a simple hydrodynamic model, i.e., Stoke's law. In this model the friction matrix is given by,¹⁷

$$\gamma_{ij} = \delta_{ij} \cdot 6\pi a_i \eta / m_i \quad (28)$$

where η is the solvent viscosity and a_i is the hydrodynamic radius of atom i . Equation 28 is derived using the linear Navier–Stokes equation by calculating the force exerted on a sphere of a given hydrodynamic radius, moving at constant velocity in a

fluid of constant viscosity. The hydrodynamic radius can be estimated from the solvent accessible surface area, s , the radius of probe (which corresponds to the radius of water molecule), r_p , and van der Waals radius, r_{vdW} , as follows,^{10,18}

$$a_i = r_{\text{vdW},i} \sqrt{\sigma_i / 4\pi / (r_{\text{vdW}} + r_p)^2} \quad (29)$$

The Stokes' law friction in Cartesian form was calculated using eqs 28 and 29 with $\eta = 0.8$ cp (the approximate viscosity of water at 30 °C^{11,41}) and $r_p = 1.4$ Å,¹⁸ followed by transformation to normal mode representation using eq 8. Figure 4 shows that γ thus derived is nearly frequency independent. Modes of frequency $\omega < \sim 60$ cm⁻¹ are overdamped. Comparing the MD results in Figure 2 with the hydrodynamic model shows that the Stokes' law model overestimates the friction and lacks the frequency dependence. This is probably due to the lack of the anharmonic contribution arising from the interatomic correlation (i.e., the vacuum friction via the intraprotein interaction is neglected) and to the simplified treatment of solvent contribution via the ASA.¹⁹ Furthermore, in the Stokes' law model, the temperature dependence of the friction is represented only through the temperature-dependent viscosity of water,

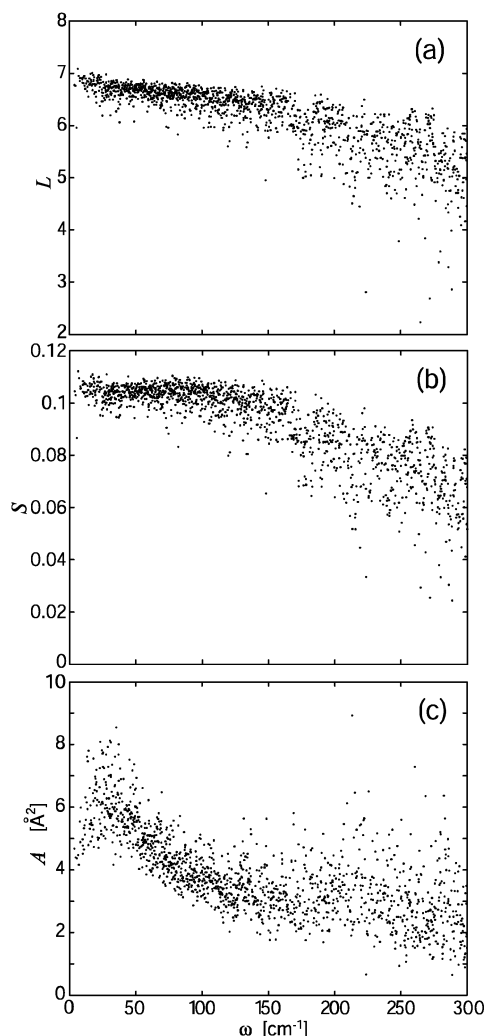


Figure 3. (a) Localization factor, L (eq 24), (b) intramolecular interaction, S (eq 26), and (c) average accessible surface area, A (eq 27), as a function of normal-mode frequency at 300 K.

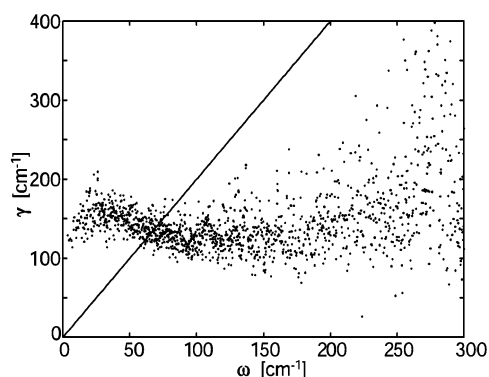


Figure 4. Diagonal friction as a function of normal-mode frequency, $\gamma(\omega)$, derived from the normal modes at 300 K combined with the Stokes' law. The solid line indicates the critical damping frequencies, i.e., the boundary between underdamped and overdamped modes at $\gamma = 2\omega$.

neglecting all other dynamical effects, such as motional frequency modification.

The modification of the curvature of the vibrational PMF from the NMA curvature, ω_{NMA} , was calculated by fitting eq 9 to the MD-derived velocity-autocorrelation function of each normal mode, thus furnishing ω_{vacuum} from the MD in vacuum and ω_{water} from the MD in water. To obtain a physical understanding of this frequency, the vibrational density of states from the MD

simulation, calculated using the individual normal-mode displacement vectors, was compared with that of the Langevin model. To do this, the vibrational spectrum of the n th normal mode, $g_n(\omega)$, was calculated by Fourier transformation of the normal-mode velocity-autocorrelation function, $\langle \dot{Q}_n(0)\dot{Q}_n(t) \rangle$, obtained from the trajectories of the mass-weighted Cartesian velocities, $\mathbf{v}(t)$ (in eq 5) via $\dot{Q}_n(t) = \mathbf{v}(t) \cdot \mathbf{u}_n$. The Langevin vibrational spectrum with γ_{nm} and ω_n is given in the summation of the right side of eq 22, i.e., $\gamma_{nm}\omega^2/\pi\{(\omega^2 - \omega_n^2) + \gamma_{nm}^2\omega^2\}$. Figure 5a indicates a good agreement, although the MD-derived spectrum is somewhat broad because of the complex anharmonicity. The frequency derived by the VACF fitting procedure can be thus considered as representative of the vibrational motion along the normal mode.

The frequency shift from ω_{NMA} arises from two contributions: the intraprotein interaction, $(\omega_{\text{vacuum}} - \omega_{\text{NMA}})/\omega_{\text{NMA}}$, and solvation, $(\omega_{\text{water}} - \omega_{\text{vacuum}})/\omega_{\text{NMA}}$. These two contributions are shown in Figure 5b and c. In the vacuum MD, the frequencies are lower relative to the normal modes, indicating PES broadening via anharmonicity. The magnitude of the frequency shift increases with increasing temperature and decreasing frequency. Interestingly, in water, the MD frequencies increase relative to in vacuum. The spectra in Figure 5a show that this increase occurs over the whole frequency range. The PES curvatures become steeper because of the confinement of the protein atoms due to interaction with the surrounding water molecules.^{11,12,42} The lower-frequency modes, which have relatively large accessible surface areas, A , undergo large frequency shifts. The shifts to high frequency at 120 K are comparable to those at 300 K, implying that the solvent contribution to the vibrational PMF is relatively temperature independent, i.e., the protein-atom confinement by the surrounding waters is determined by the water-molecule static equilibrium positions. In contrast, temperature has a strong influence on the magnitude of the friction itself, which is thus determined by the dynamic fluctuations of the water molecules.

3.1.2. Model Functions of Diagonal Friction and Potential of Mean Force. We now construct a phenomenological model function for the diagonal friction. For this purpose, we first assume that γ of each mode is determined by both the frequency and the quantities S (in eq 26) and A (in eq 27), which are determined by the displacement vectors, i.e., $\gamma = \gamma(\omega, S, A)$. Moreover, the origin of the friction is assumed to be decomposable into contributions from intraprotein interaction and solvation. The contribution from intraprotein interaction is assumed to be determined by the vacuum MD. To calculate this, γ_{vacuum} is modeled using the intraprotein interaction parameter, S . The solvation contribution is characterized by the relative friction increase going from vacuum to water, $(\gamma_{\text{water}} - \gamma_{\text{vacuum}})/\gamma_{\text{vacuum}}$, parametrized as a function of the accessible surface area, A . Thus, model functions of both γ_{vacuum} and $(\gamma_{\text{water}} - \gamma_{\text{vacuum}})/\gamma_{\text{vacuum}}$ were constructed.

The collective motions of $\omega < 100 \text{ cm}^{-1}$ have similar values of S and A , in contrast to the large variations in these quantities observed for the higher frequency vibrations in Figure 3, indicating similarity of their global characteristics. Therefore, the friction coefficients associated with the collective motions are characterized largely by their frequencies. For this reason, the model functions were separated into two frequency regions, $\omega < 100 \text{ cm}^{-1}$ and $\omega = 100\text{--}300 \text{ cm}^{-1}$. The fitted model functions are as follows, with both the frequency and the friction in units of cm^{-1} , and A in units of \AA^2 . At 120 K:

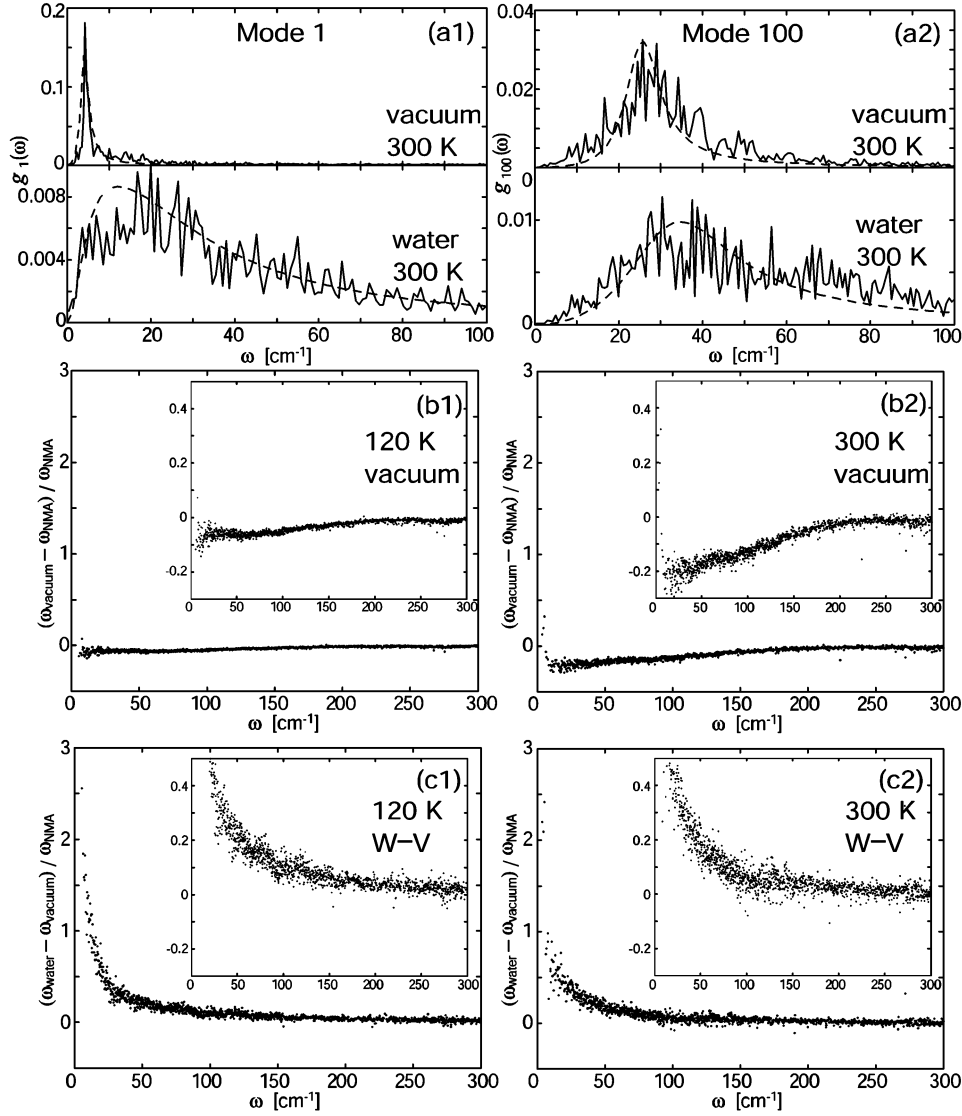


Figure 5. (a) Vibrational density of states from MD at 300 K in vacuum and in water along each normal mode. (1) Mode 1 ($\omega_{\text{NMA}} = 12.2 \text{ cm}^{-1}$) and (2) mode 100 ($\omega_{\text{NMA}} = 34.7 \text{ cm}^{-1}$). Those from the Langevin model with MD-derived parameters are also shown by dashed curves. In (b) and (c) are shown the frequency shifts of the harmonic potential of mean force: (b) $(\omega_{\text{vacuum}} - \omega_{\text{NMA}})/\omega_{\text{NMA}}$ and (c) $(\omega_{\text{water}} - \omega_{\text{vacuum}})/\omega_{\text{NMA}}$. Results are shown from (1) MD at 120 K and (2) MD at 300 K. The results are plotted on an enlarged scale in the insets.

$$\gamma_{\text{vacuum}} \approx \begin{cases} 2.8S\omega^{0.8} & \omega < 100 \text{ cm}^{-1} \\ 110S & \omega \geq 100 \text{ cm}^{-1} \end{cases} \quad (30)$$

$$\frac{\gamma_{\text{water}} - \gamma_{\text{vacuum}}}{\gamma_{\text{vacuum}}} \approx \begin{cases} 14A/\omega + 0.8 & \omega < 100 \text{ cm}^{-1} \\ 0.24A + 0.4 & \omega \geq 100 \text{ cm}^{-1} \end{cases} \quad (31)$$

At 300 K:

$$\gamma_{\text{vacuum}} \approx \begin{cases} 9.6S\omega^{0.8} & \omega < 100 \text{ cm}^{-1} \\ 440S & \omega \geq 100 \text{ cm}^{-1} \end{cases} \quad (32)$$

$$\frac{\gamma_{\text{water}} - \gamma_{\text{vacuum}}}{\gamma_{\text{vacuum}}} \approx \begin{cases} 5.9A/\omega + 1.0 & \omega < 100 \text{ cm}^{-1} \\ 0.33A + 0.1 & \omega \geq 100 \text{ cm}^{-1} \end{cases} \quad (33)$$

Table 1 shows the correlation coefficients between the model and MD-derived frequency-dependent frictions. The correlation is satisfactory for $\omega < 100 \text{ cm}^{-1}$ at both 120 and 300 K, but less so for $\omega \geq 100 \text{ cm}^{-1}$. In Figure 6a is plotted the friction

TABLE 1: Correlation Coefficients between the MD-Derived and Model Frictions

	γ_{vacuum} 0–100 cm^{-1}	γ_{vacuum} 100–300 cm^{-1}	$(\gamma_{\text{water}} - \gamma_{\text{vacuum}})/\gamma_{\text{vacuum}}$ 0–100 cm^{-1}	$(\gamma_{\text{water}} - \gamma_{\text{vacuum}})/\gamma_{\text{vacuum}}$ 100–300 cm^{-1}
120 K	0.93	0.21	0.85	0.39
300 K	0.97	0.18	0.86	0.43

from the model equations of eqs 30–33. Although the MD frictions are more widely spread than that of the model friction, these simple model functions reproduce well the average frequency dependence of the MD-derived frictions, γ_{water} and γ_{vacuum} in Figure 2a.

We also derive here phenomenological model functions for the shifts of the frequencies from the harmonic, normal mode values. To do this, we assume that the frequency shifts relative to the NMA are less dependent on the geometrical form of the normal modes but rather are a function of only the NMA frequency. $(\omega_{\text{vacuum}} - \omega_{\text{NMA}})/\omega_{\text{NMA}}$ and $(\omega_{\text{water}} - \omega_{\text{vacuum}})/\omega_{\text{NMA}}$ are separately modeled to again separate the contributions from intraprotein interaction and solvation. The resulting model

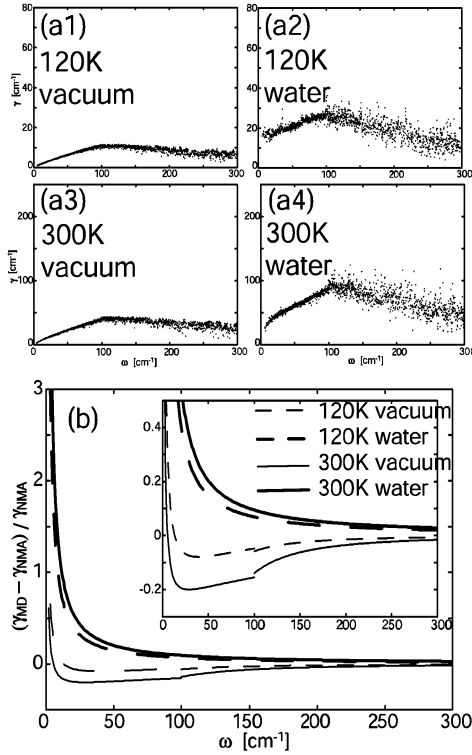


Figure 6. (a) Diagonal friction as a function of normal-mode frequency, $\gamma(\omega)$, calculated using the model functions of eqs 30–33. (1) MD in vacuum at 120 K, (2) MD in water at 120 K, (3) MD in vacuum at 300 K, and (4) MD in water at 300 K. (b) The model functions of the frequency shift of PMF in eqs 34–37: $(\omega_{\text{vacuum}} - \omega_{\text{NMA}})/\omega_{\text{NMA}}$ at 120 K (dashed curve) and at 300 K (solid curve), and $(\omega_{\text{water}} - \omega_{\text{vacuum}})/\omega_{\text{NMA}}$ at 120 K (thick solid curve) and at 300 K (thick solid curve).

functions are shown as follows with the frequency in units of cm^{-1} . At 120 K:

$$\frac{\omega_{\text{vacuum}} - \omega_{\text{NMA}}}{\omega_{\text{NMA}}} = \begin{cases} 0.58\omega_{\text{NMA}}^{0.1} + 3.3\omega_{\text{NMA}}^{-1} - 1 & \omega < 100 \text{ cm}^{-1} \\ -580/\omega_{\text{NMA}}^2 & \omega \geq 100 \text{ cm}^{-1} \end{cases} \quad (34)$$

$$\frac{\omega_{\text{water}} - \omega_{\text{vacuum}}}{\omega_{\text{NMA}}} = 15/\omega_{\text{NMA}}^{1.1} \quad (35)$$

At 300 K:

$$\frac{\omega_{\text{vacuum}} - \omega_{\text{NMA}}}{\omega_{\text{NMA}}} = \begin{cases} 0.52\omega_{\text{NMA}}^{0.1} + 2.1\omega_{\text{NMA}}^{-1} - 1 & \omega < 100 \text{ cm}^{-1} \\ -1400/\omega_{\text{NMA}}^2 & \omega \geq 100 \text{ cm}^{-1} \end{cases} \quad (36)$$

$$\frac{\omega_{\text{water}} - \omega_{\text{vacuum}}}{\omega_{\text{NMA}}} = 11/\omega_{\text{NMA}}^{1.1} \quad (37)$$

Table 2 shows the correlation coefficients between the model functions and the MD frequencies. This, together with Figures 5b,c and 6b demonstrates that, again, the model functions adequately reproduce the simulation-derived frequencies.

Finally, we discuss the physical interpretation of the model functions with reference to the potential energy landscape. The anharmonicity via intraprotein interaction broadens the curvature of the PMF relative to the NMA parabola. In contrast, the interaction of the protein with the surrounding water molecules

TABLE 2: Correlation Coefficients between the MD-Derived and Model Frequencies

	$(\omega_{\text{vacuum}} - \omega_{\text{NMA}})/\omega_{\text{NMA}}$ 0–100 cm^{-1}	$(\omega_{\text{vacuum}} - \omega_{\text{NMA}})/\omega_{\text{NMA}}$ 100–300 cm^{-1}	$(\omega_{\text{water}} - \omega_{\text{vacuum}})/\omega_{\text{NMA}}$ 0–300 cm^{-1}
120 K	0.85	0.88	0.97
300 K	0.83	0.93	0.93

leads to confinement of the protein atoms, resulting in steeper potential energy wells. With regard to the friction, which is related to the roughness within a single potential well in a vacuum, this is proportional to the anharmonic intraprotein interaction, S , and in solution to the accessible surface area, A , which determines the damping resulting from collisions with the water molecules. In the case of the low-frequency collective motions, interestingly, γ_{vacuum} decreases and $(\gamma_{\text{water}} - \gamma_{\text{vacuum}})/\gamma_{\text{vacuum}}$ increases with decreasing ω_{NMA} . This frequency dependence can be explained via the coupling of two motions, which is related to the overlap of their vibrational densities of states, owing to frequency resonance.⁴³ With decreasing frequency, the collective protein motions are more likely to decouple from high-frequency protein vibrations (via decreasing overlap of vibrational density of states with increasing the gap in frequency between the collective motions and high-frequency protein vibrations) and, in contrast, more likely to couple to the longer-time scale motions of the water molecules such as translation and reorientation.

3.1.3. Off-Diagonal Friction. The off-diagonal parts of the friction matrix calculated from the MD simulations are now examined. The off-diagonal friction originates from anharmonicity in the potential energy surface, leading to the coupling of modes, i.e., mode–mode interaction.

The average over the absolute value of the off-diagonal frictions, $|\gamma_{nm}|$, with frequencies, $\omega_n, \omega_m < 100 \text{ cm}^{-1}$, is 0.134 and 0.362 cm^{-1} at 120 K in vacuum and in water, respectively, and 0.544 and 1.03 cm^{-1} at 300 K in vacuum and in water, respectively. Thus, the off-diagonal friction is larger at 300 K than at 120 K and larger in water than in vacuum because of stronger anharmonicity at higher temperature and the solvent friction, respectively. However, the off-diagonal friction is much smaller than the diagonal friction, for which the averages are 7.05 and 22.0 cm^{-1} at 120 K in vacuum and in water, respectively, and 24.9, and 63.5 cm^{-1} at 300 K in vacuum and in water, respectively.

The dependence of the off-diagonal friction matrix elements on the frequencies and atomic displacement vectors of any given pair of modes was examined in a manner similar to the diagonal friction. The vacuum friction originates from the mode–mode interaction, which is parametrized by S_{nm} in eq 25. Figure 7a shows $|\gamma_{nm,\text{vacuum}}|$ plotted against S_{nm} . The off-diagonal friction increases with S_{nm} . Further, two types of frequency dependence were found. First, Figure 7b, in which $|\gamma_{nm,\text{vacuum}}|$ is plotted against $\bar{\omega}_{nm} \equiv |\omega_n + \omega_m|/2$, shows that off-diagonal friction increases with $\bar{\omega}_{nm}$. Second, Figure 7c, in which $|\gamma_{nm,\text{vacuum}}|$ is plotted against $\Delta\omega_{nm} \equiv |\omega_n - \omega_m|$, shows that the off-diagonal friction becomes larger as the gap in frequency between the two modes, $\Delta\omega_{nm}$, decreases. With regard to the solvent contribution, $A_{nm} \equiv \sum_i \sigma_i |\mathbf{u}_n^{(i)} \cdot \mathbf{u}_m^{(i)}|$ can be defined analogously to eq 26 so as to quantify the ASA of a pair of modes. In Figure 7d $|\gamma_{nm,\text{water}}| - |\gamma_{nm,\text{vacuum}}|$ is plotted against A_{nm} , demonstrating that the accessible surface area is highly correlated with the increase of the off-diagonal friction via solvation.

The above off-diagonal friction results can be explained physically as follows. The coupling of a pair of modes through the off-diagonal friction increases in proportion to the mode–

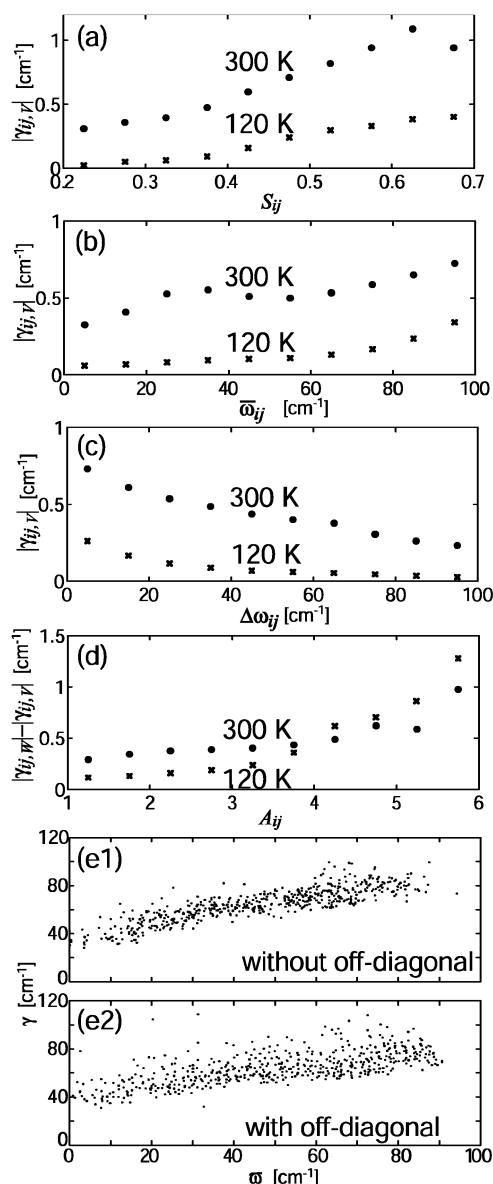


Figure 7. (a–c) Absolute value of the vacuum-MD friction at 120 K (cross) and at 300 K (dot) is shown as a function of S_{nm} , $\bar{\omega}_{nm}$, and $\Delta\omega_{nm}$, respectively. (d) The difference of the absolute value between the water friction and the vacuum friction at 120 K (cross) and at 300 K (dot) is shown as a function of A_{nm} . In (a–d), bins with 0.05 cm^{-1} , 10 cm^{-1} , 10 cm^{-1} , and 0.5 \AA^2 widths are constructed, respectively, allowing the average of the frictions within the same bin to be plotted. (e) Effective frequency and friction of the Langevin mode analysis from MD at 300 K in water: (1) without the off-diagonal friction and (2) with the off-diagonal friction.

mode interaction, S_{nm} , and to the ASA, A_{nm} , i.e., the area colliding with the water molecules. The anharmonic coupling between two low-frequency, collective protein motions is mediated by the high-frequency protein vibrations analogously to the low-frequency diagonal friction. This coupling is likely to be higher with increasing average frequency of the low-frequency modes, $\bar{\omega}_{nm} \equiv |\omega_n + \omega_m|/2$, i.e., with increasing overlap between the low- and high-frequency protein vibrational densities of states.⁴³ A pair of modes with a smaller frequency gap, $\Delta\omega_{nm} \equiv |\omega_n - \omega_m|$, thus undergoes a higher coupling in accordance with frequency resonance.^{40,44–46}

The calculation of the off-diagonal friction allows the accuracy of the diagonal-friction approximation to be examined. Knowledge of the full matrix of \mathbf{B} in eq 5 makes possible the

calculation of the eigenvalues, $\lambda_n = -\gamma_n/2 \pm \varpi_n$ for underdamped modes and $\lambda_n = -\gamma_n/2 \pm \varpi_{0n}$ for overdamped modes. Equation 6 indicates that the eigenvalues contain the information of phase space time-correlation functions. To evaluate the contribution of the off-diagonal friction, the eigenvalues of the Langevin modes with the full friction matrix were compared with those obtained using the diagonal-friction approximation. This comparison is possible only for the underdamped modes, as the negative real eigenvalues of the overdamped modes derived via diagonalizing \mathbf{B} cannot be decomposed into frequency and frictional contributions. Figure 7e shows that the distribution of underdamped eigenvalues (with the friction as the real part: vertical axis, and the effective frequency as the imaginary part: horizontal axis) is similar when calculated using the full friction matrix and when using only the diagonal friction. This similarity was found at both temperatures examined and both in vacuum and in solution (results not shown). Therefore, we conclude that the off-diagonal friction can be treated simply as a higher-order perturbation of the diagonal part and can be neglected for the present purposes.

3.2. Dynamic Structure Factor and Vibrational Density of States. We now examine the dynamic structure factor and the vibrational density of states. We compare spectra of these quantities derived directly from the MD simulations with spectra calculated using the Langevin model. The spectra calculated from the Langevin model are derived in two ways: using the MD-derived parameters and using the model-function parameters. The off-diagonal friction, which was shown in Section 3.1.3 to be very small, is neglected.

In Figure 8a and b are shown the dynamic structure factor, $S(q, \omega)$, calculated directly from the vacuum and solution MD simulations at 120 K and at 300 K using eq 17 and from the Langevin model with the MD-derived friction and frequency using eq 19. The Langevin description roughly reproduces the spectra from the MD trajectories. The variation with temperature and solvation are also well reproduced.

The effects of solvation and temperature on the MD spectra can be analyzed with the Langevin model, decomposing the spectra into the contributions from each mode¹⁶ (as is shown in eqs 19 and 20). The surrounding water molecules lead to a decrease of the inelastic, lower-frequency vibrational intensity ($\hbar\omega = 0.5\text{--}10 \text{ meV}$) and an increase of quasielastic intensity ($\hbar\omega = 0.1\text{--}0.5 \text{ meV}$) in contrast to the higher-frequency vibrational intensity ($\hbar\omega > 10 \text{ meV}$), which varies little. Thus, the solvent molecules around the protein reduce the lower-frequency vibrational amplitudes and enhance the diffusive motion,^{11,12,42} consistent with the frequency-dependent increase of the friction analyzed in Section 3.1.1. In other words, the large friction increases in the low-frequency modes enhance diffusive motions (not clearly seen in the Langevin spectra but shown in the MD spectra) and thus increase the quasielastic intensity as well as decreasing the vibrational, inelastic intensity, while the small friction increase in the high-frequency modes results in little change in the higher-frequency intensity. In contrast to the behavior at 300 K, diffusion is not significantly enhanced by the friction increase at 120 K probably attributable to the potential energy landscape being more harmonic at this temperature.

The spectra from the Langevin model underestimate the quasielastic intensity ($\hbar\omega = 0.1\text{--}0.5 \text{ meV}$). Therefore, for the full reproduction of the spectra, a further diffusive contribution should be added to the Langevin model. To do this, a corrected intermediate scattering function F_{corr} is assumed to be factorizable as the product of that of the Langevin model, F_L , and

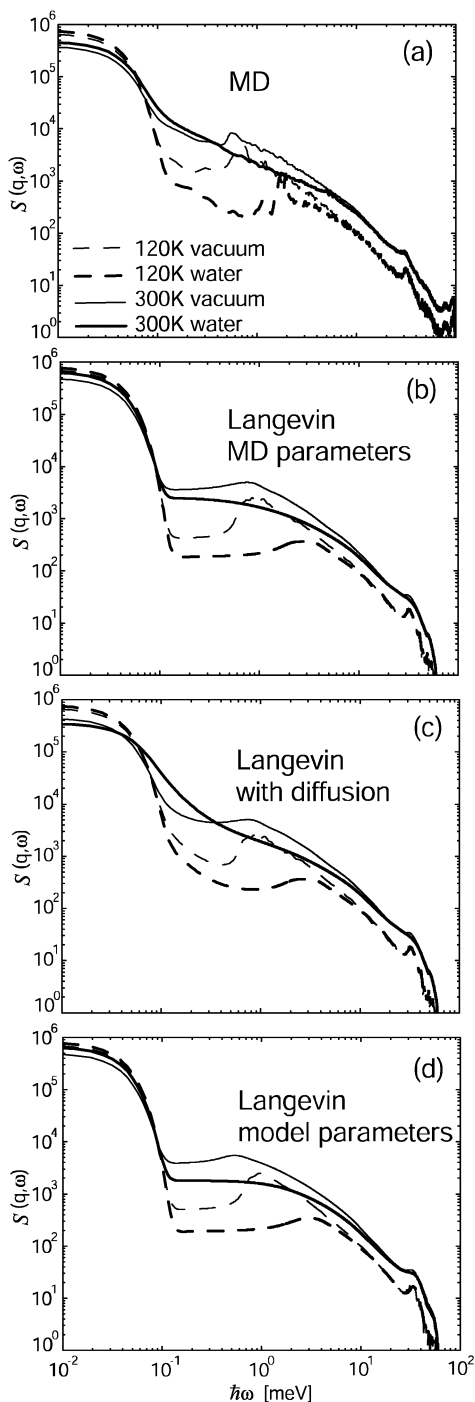


Figure 8. Dynamic structure factor, $S(q, \omega)$, at $q = 2 \text{ \AA}^{-1}$ (see text), derived (a) from MD trajectory, (b) from Langevin model with the MD-derived parameters, (c) the same as (b) but including the diffusive correction in eq 38, and (d) from Langevin model with the model parameters. Spectra are shown from MD in vacuum at 120 K (dashed curve), from MD in water at 120 K (thick dashed curve), from MD in vacuum at 300 K (solid curve), and from MD in water at 300 K (thick solid curve).

that of the additional contribution F_D , the latter being calculated assuming simple translational diffusion with diffusion constant, D , i.e.,

$$F_{\text{cor}}(q, t) \approx F_L(q, t)F_D(q, t) \quad (38)$$

where $F_D(q, t) = \exp(-Dq^2t)$.

The diffusion constant derived from the Langevin model is zero because the diffusion constant of each mode n , d_n , is $d_n =$

$\int_0^\infty \langle v_n(0)v_n(t) \rangle dt = 0$, as can be derived from the velocity-autocorrelation function in eq 9. This arises from the assumption that the potential energy is harmonic in eq 3. Therefore, the diffusion constant for the correction of the spectra was calculated directly from the MD trajectory.

Using the MD trajectory, the required diffusion constant can be obtained from the mean-square displacement calculated as a function of time. To determine D in a manner consistent with the scattering-length weighted definition in the intermediate scattering function of eq 18, the mean-square displacement was scattering-length weighted as follows.

$$\langle r^2(t) \rangle = \sum_{i=1}^N b_{\text{inc},i}^2 \langle |\mathbf{r}_i(t) - \mathbf{r}_i(0)|^2 \rangle / \sum_{i=1}^N b_{\text{inc},i}^2 \quad (39)$$

D was calculated from the gradient of $\langle r^2(t) \rangle$ over the range $t = 200\text{--}500$ ps by linear regression, resulting in $D = 3.1 \times 10^{-4}$, 3.2×10^{-4} , 7.1×10^{-3} , and $4.2 \times 10^{-2} [\text{\AA}^2/\text{ps}]$ at 120 K in a vacuum and in water, and at 300 K in vacuum and in water, respectively.

In Figure 8c the corrected spectra are shown, calculated by the Fourier transformation of the intermediate scattering function in eq 38. The diffusion-corrected Langevin model excellently reproduces the spectra.

The vibrational density of states, $g(\omega)$, for the four simulation conditions were calculated from the MD simulations (eq 21) and, alternatively, from the Langevin model with the MD-derived frictions and frequencies (eq 22). Figure 9a and b show that $g(\omega)$ calculated with these two methods agrees well again, demonstrating the validity of the Langevin model. At both temperatures, solvent shifts the spectra to higher frequencies, i.e., it reduces the intensity at $\omega < \sim 50 \text{ cm}^{-1}$ and enhances the mode density at higher frequencies, $\omega > \sim 150 \text{ cm}^{-1}$. The shift to higher frequencies arises from changes of the protein potential energy surface because of due to confinement by the water molecules^{11,12,42} and is also apparent in the Langevin model parameters. As well as the increase of the vibrational PMF, i.e., the shift to high-frequencies of their equilibrium vibrational frequencies, the specific friction increases in the lower-frequency vibrations, leading to broadening of their spectral intensities¹⁶ and thus decreasing their peak amplitudes in the vibrational, inelastic scattering region while increasing the quasielastic intensity (which is not observed clearly in the inelastic, vibrational spectra, $g(\omega)$). However, the temperature dependence, seen in the spectra computed from the MD, i.e., the increase of lower-frequency intensity $< \sim 50 \text{ cm}^{-1}$ with increasing temperature, is not clearly reproduced in the Langevin-derived spectra. This probably arises from the insufficiency of the Langevin model in describing certain slow motions, as was discussed above in the section on the dynamic structure factor.

Finally, we examine whether the model function of the friction (eqs 30–33) and the frequency (eqs 34–37) can adequately represent the dynamic structure factor and the vibrational density of states. Figures 8d and 9c show the corresponding $S(q, \omega)$ and $g(\omega)$. These spectra are in excellent agreement with the spectra calculated using the Langevin model with MD-derived parameters. There are some differences in the high-frequency regions of $g(\omega)$ probably attributable to the simplicity of the friction model function, which lacks the width of the friction distribution, $\Delta\gamma$, in the high-frequency region. However, the model parameters reproduce qualitatively the solvent effects of both the damping of high-frequency motions and the enhancement of low-frequency motions, and their temperature dependence.

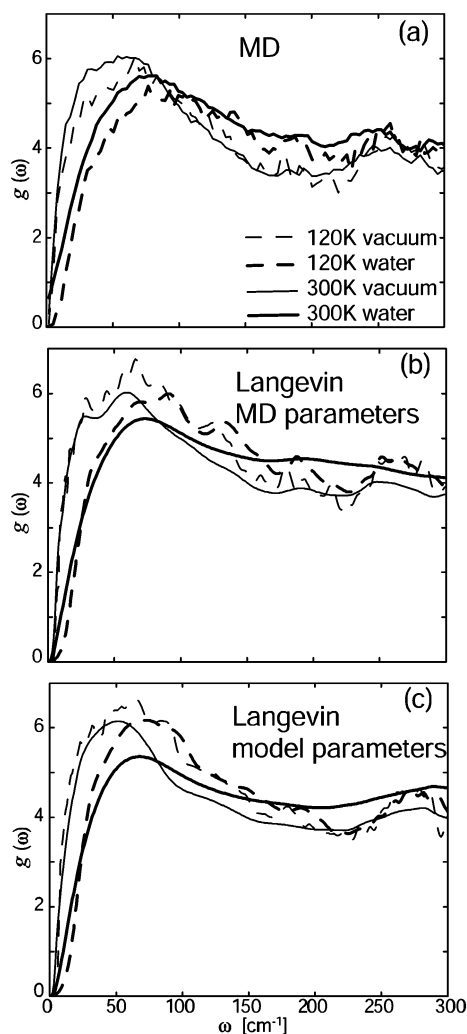


Figure 9. Vibrational density of states, $g(\omega)$, derived (a) from MD trajectory, (b) from Langevin model with the MD-derived parameters, and (c) from Langevin model with the model parameters. Spectra are shown from MD in vacuum at 120 K (dashed curve), from MD in water at 120 K (thick dashed curve), from MD in vacuum at 300 K (solid curve) and from MD in water at 300 K (thick curve).

4. Conclusion

In the work presented here, a simplified description of the internal vibrational dynamics of myoglobin has been obtained in terms of the friction matrix and the harmonic potential of mean force (PMF), as derived from Langevin mode analysis applied to molecular dynamics trajectories. The resulting friction matrix and the PMF were subsequently modeled using parametrized phenomenological functions and thus physically interpreted.

The diagonal parts of the friction matrix on the normal mode basis were modeled as a function of frequency and certain quantities that are determined by the atomic displacement vectors. Although the model functions derived are too simple to follow details of the MD-derived friction distribution, the average frequency dependence is well reproduced. For the local high-frequency vibrations, the friction is determined by the magnitude of the intraprotein interaction, S , and collisions with water molecules as parametrized by the accessible surface area, A . The frictional effects on the collective, low-frequency motions are more highly frequency dependent, implying the coupling of the collective protein motions both to the slow, translational, and reorientational water motions and to protein high-frequency

vibrations. The degree of this coupling depends on the magnitude of the overlap of the vibrational densities of states.⁴³

The frequency obtained from the VACF fitting corresponds to the mean quadratic potential curvature of individual conformational substates sampled by MD simulations. The anharmonicity due to intraprotein interaction is found here to broaden the curvature of the PMF relative to the harmonic normal-mode frequency. This shift to lower frequencies is larger at 300 K than at 120 K, and also larger for the lower-frequency normal modes, which are thus more anharmonic. In contrast, the interactions with surrounding water molecules reduce the vibrational fluctuations in the protein molecule, as evidenced by a shift to higher frequencies. The lower-frequency modes, with relatively large accessible surface areas, undergo larger frequency shifts. This confinement by the surrounding waters is determined mostly by their equilibrium static positions and is thus relatively temperature independent. The surrounding waters enhance diffusional motions, in contrast to their effect in suppressing vibrational fluctuations. This diffusion enhancement is deduced to originate from the increased friction by solvation.

The off-diagonal elements of the friction matrix are also determined here, as a function of both the normal-mode frequencies and atomic displacement vectors. Although this dependence is too complicated to allow construction of a simple model function, it is found that the coupling of two low-frequency modes through off-diagonal friction becomes higher as the gap in frequency between the two modes increases, via resonance,^{40,44–46} as well as with increasing the mode–mode interaction and with increasing the average frequency of two modes, as the effect is again likely to arise from the overlap of their densities of states with those of the higher-frequency protein vibrations.⁴³ Solvation also increases the magnitude of the coupling, in a manner depending on the ASA.

The off-diagonal elements are shown to be small enough to allow the approximation of diagonal friction on the normal mode basis to be useful. The same approximation on the Cartesian coordinate basis may also be assumed.¹⁵ These two approximations for the Langevin friction are likely to have similar accuracies, i.e., the ratios of the off-diagonal to diagonal elements may be similar. Of the two, the normal-mode description has certain advantages in representing protein dynamics simply. Furthermore, the approximation on the normal-mode basis is applicable straightforwardly in the derivation of the intermediate scattering function (eqs 19 and 20).

The validity of the Langevin model that uses the model functions of Langevin parameters was tested by further comparisons involving the dynamic structure factor and the vibrational density of states. It is found that the MD-derived spectra can be largely reproduced in terms of the atomic-resolution normal modes combined with the model functions of both the friction and the potential of mean force. However, the slow, diffusive motions in the quasielastic region are absent in the Langevin model. The subsequent addition of a diffusive contribution, applied here using the diffusion constant obtained from the MD mean-square displacement, makes possible the reproduction of the full quasielastic intensity of the MD dynamic structure factor. The absence of the slow, diffusive contribution in the Langevin model is most likely due to the harmonic approximation of the potential energy used here. The Langevin parameters obtained from the velocity-autocorrelation function are relatively insensitive to the slow and infrequent barrier-crossing motions between conformational substates and rather represent the vibrational motion averaged over the potential

wells explored. In this sense, the present Langevin model is an appropriate simplified description of protein vibrational dynamics, i.e., the friction coefficients obtained by the Langevin model pertain to the local roughness of the PES within the potential wells explored by the system.

The Langevin description can be further developed in several directions. One is to introduce a multimimum free energy surface directly into $V(\mathbf{q})$ in eq 1 using, for example, principal component analysis.^{4–8} In this way, diffusive, barrier-crossing dynamics can be directly incorporated. A second development would be to use a more advanced model of the friction, such as that contained in the generalized Langevin model.^{47,48} Application of the generalized Langevin model to principal component modes may enable introduction of slow, diffusive motions arising from the memory effect of the friction kernel. The temperature dependence of the friction (friction kernel) in this type of model would also be of interest.

Use of the present model functions of the friction and PMF allows the dynamic structure factor and the vibrational density of states to be obtained directly from the frequencies and displacement vectors of protein normal modes. The understanding and modeling of the equilibrium potential curvature via mode coupling and solvent effects thus obtained may also be useful in the assignment of peaks in vibrational spectroscopy. For example, the simplified representation of protein vibrational dynamics by the Langevin model, using normal modes combined with the model parameters of friction and frequency via their frequencies and their atomic displacement vectors, can serve in the analysis of protein high-resolution vibrational neutron scattering spectra, such as have been obtained in recent years.^{49,50}

Finally, the characterization of frictional effects obtained here should be useful in understanding mechanism of chemical- and light-induced energy dissipation through solvent-modified vibrational coupling in protein.^{40,45,46,51–60}

Acknowledgment. We thank G. R. Kneller for helpful comments. K.M. acknowledges a research fellowship of the Japan Society for the Promotion of Science for young scientists.

References and Notes

- Frauenfelder, H.; Slinger, S. G.; Wolynes, P. G. *Science* **1991**, *254*, 1598.
- Frauenfelder, H.; Parak, F.; Young, R. D. *Annu. Rev. Biophys. Chem.* **1988**, *17*, 451.
- Karplus, M.; McCammon, J. A. *Nat. Struct. Biol.* **2002**, *9*, 646.
- Amadei, A.; Linssen, A. B. M.; Berendsen, H. J. C. *Proteins: Struct., Funct., Genet.* **1993**, *17*, 283.
- de Groot, B. L.; van Aalten, D. M. F.; Amadei, A.; Berendsen, H. J. C. *Biophys. J.* **1996**, *71*, 1707.
- Kitao, A.; Hayward, S.; Gō, N. *Proteins: Struct., Funct., Genet.* **1998**, *33*, 496.
- Kitao, A.; Go, N. *Curr. Opin. Struct. Biol.* **1999**, *9*, 164.
- Tournier, A. L.; Smith, J. C. *Phys. Rev. Lett.* **2003**, *91*, 208106.
- Lamm, G.; Szabo, A. J. *Chem. Phys.* **1986**, *85*, 7334.
- Kottalam, J.; Case, D. A. *Biopolymers* **1990**, *29*, 1409.
- Kitao, A.; Hirata, F.; Gō, N. *Chem. Phys.* **1991**, *158*, 447.
- Hayward, S.; Kitao, A.; Hirata, F.; Gō, N. *J. Mol. Biol.* **1993**, *234*, 1207.
- Ansari, A. J. *Chem. Phys.* **1999**, *110*, 1774.
- Kneller, G. R. *Chem. Phys.* **2000**, *261*, 1.
- Hinsen, K.; Petrescu, A. J.; Dellerue, S.; Bellissent-Funel, M. C.; Kneller, G. R. *Chem. Phys.* **2000**, *261*, 25.
- Smith, J. C.; Cusack, S.; Tidor, B.; Karplus, M. *J. Chem. Phys.* **1990**, *93*, 2974.
- Chandrasekhar, S. *Rev. Mod. Phys.* **1943**, *15*, 1.
- Paster, R. W.; Karplus, M. *J. Phys. Chem.* **1988**, *92*, 2636.
- Feig, M.; Brooks, C. L., III. *Curr. Opin. Struct. Biol.* **2004**, *14*, 217.
- Tournier, A. L.; Xu, J.; Smith, J. C. *Biophys. J.* **2003**, *85*, 1871.
- Parak, F.; Formanek, H. *Acta Crystallogr., Sect. A* **1971**, *27*, 573.
- Iben, I. E.; Braunstein, D.; Doster, W.; Frauenfelder, H.; Hong, M. K.; Johnson, J. B.; Luck, S.; Ormos, P.; Schulte, A.; Steinbach, P. J.; Xie, A. H.; Young, R. D. *Phys. Rev. Lett.* **1989**, *62*, 1916.
- Doster, W.; Cusack, S.; Petry, W. *Nature* **1989**, *337*, 754.
- Vojtechovsky, R.; Chu, K.; Berendsen, J.; Sweet, R. M.; Schlichting, I. *Biophys. J.* **1999**, *78*, 2752.
- Brooks, B. R.; Brucoleri, R. E.; Olafson, B. D.; States, D. J.; Swaminathan, S.; Karplus, M. *J. Comput. Biol.* **1983**, *4*, 187.
- MacKerell, A. D., Jr.; Bashford, D.; Bellott, R. L.; Dunbrack, R. L., Jr.; Evanseck, J. D.; Field, M. J.; Fischer, S.; Gao, J.; Guo, H.; Ha, S.; Joseph-McCarthy, D.; Kuchnir, L.; Kuczera, K.; Lau, F. T. K.; Mattos, C.; Michnick, S.; Ngo, T.; Nguyen, D. T.; Prodhom, B.; Reiher, W. E., III; Roux, B.; Schlenkrich, M.; Smith, J. C.; Stote, R.; Straub, J.; Watanabe, M.; Wiorkiewicz-Kuczera, J.; Yin, D.; Karplus, M. *J. Phys. Chem. B* **1998**, *102*, 3586.
- Jorgensen, W. D.; Chandrasekhar, J.; Madura, J. D. *J. Chem. Phys.* **1983**, *79*, 926.
- Nošé, S. *Mol. Phys.* **1984**, *52*, 255.
- Hoover, W. G. *Phys. Rev. A* **1985**, *31*, 1695.
- Darden, T. A.; York, D. M.; Pederson, L. G. *J. Chem. Phys.* **1993**, *98*, 10089.
- Essmann, U.; Perera, L.; Berkowitz, M. L.; Darden, T. A.; Pederson, L. G. *J. Chem. Phys.* **1995**, *103*, 8577.
- van Gunsteren, W. F.; Berendsen, H. J. C. *Mol. Phys.* **1977**, *34*, 1311.
- van Hove, L. *Phys. Rev.* **1954**, *95*, 249.
- Kneller, G. R.; Smith, J. C. *J. Mol. Biol.* **1994**, *242*, 181.
- Hayward, J. A.; Smith, J. C. *Biophys. J.* **2002**, *82*, 1216.
- Hayward, J. A.; Finny, J. L.; Daniel, R. M.; Smith, J. C. *Biophys. J.* **2003**, *85*, 679.
- Diehl, M.; Doster, W.; Petry, W.; Schöber, H. *Biophys. J.* **1997**, *73*, 2726.
- Robertson, G. N.; Yarwood, J. *Chem. Phys.* **1978**, *32*, 267.
- Balog, E.; Becker, T.; Oettl, M.; Lechner, R.; Daniel, R.; Finney, J.; Smith, J. C. *Phys. Rev. Lett.* **2004**, *93*, 028103.
- Yu, X. Y.; Leitner, D. M. *J. Phys. Chem. B* **2003**, *107*, 1698.
- Stokes, R. H.; Mills, R. *International Encyclopedia of Physical Chemistry and Chemical Physics*; Pergamon Press: Oxford, 1965; Vol. 3.
- Moritsugu, K.; Kidera, A. *J. Phys. Chem. B* **2004**, *108*, 3890.
- Brooks, C. L., III; Karplus, M. *J. Mol. Biol.* **1989**, *208*, 159.
- Sakurai, J. J.; Tuan, S. F. *Modern Quantum Mechanics*, rev. ed.; Addison-Wesley: New York, 1995.
- Moritsugu, K.; Miyashita, O.; Kidera, A. *Phys. Rev. Lett.* **2000**, *85*, 3970.
- Moritsugu, K.; Miyashita, O.; Kidera, A. *J. Phys. Chem. B* **2003**, *107*, 3309.
- Mori, H. *Prog. Theor. Phys.* **1965**, *33*, 423.
- Zwanzig, R. *Annu. Rev. Phys. Chem.* **1965**, *16*, 67.
- Goupil-Lamy, A. V.; Smith, J. C.; Yunoki, J.; Parker, S. F.; Kataoka, M. *J. Am. Chem. Soc.* **1997**, *119*, 9268.
- Kataoka, M.; Kamikubo, H.; Yunoki, J.; Tokunaga, F.; Kanaya, T.; Izumi, Y.; Shibata, S. *J. Phys. Chem. Solids* **1999**, *60*, 1285.
- Martin, J. L.; Migus, A.; Poyart, C.; Lecarpentier, Y.; Astier, R.; Antonetti, A. *Proc. Natl. Acad. Sci. U.S.A.* **1983**, *80*, 173.
- Henry, E. R.; Eaton, W. A.; Hochstrasser, R. M. *Proc. Natl. Acad. Sci. U.S.A.* **1986**, *83*, 8982.
- Petrich, J. W.; Martin, J. L.; Houde, D.; Poyart, C.; Orszag, A. *Biochemistry* **1987**, *26*, 7914.
- Lingle, R., Jr.; Xu, X.; Zhu, H.; Yu, S.-C.; Hopkins, J. B. *J. Phys. Chem.* **1991**, *95*, 9320.
- Li, P.; Sage, J. T.; Champion, P. M. *J. Chem. Phys.* **1992**, *97*, 3214.
- Franzen, S.; Bohn, B.; Poyart, C.; Martin, J. L. *Biochemistry* **1995**, *34*, 1224.
- Mizutani, Y.; Kitagawa, T. *Science (Washington, D.C.)* **1997**, *278*, 443.
- Lian, T.; Lucke, B.; Kholodenko, Y.; Hochstrasser, R. M. *J. Chem. Phys.* **1997**, *98*, 11648.
- Sagnella, D. E.; Straub, J. E. *J. Phys. Chem. B* **2001**, *105*, 7057.
- Leitner, D. *Phys. Rev. Lett.* **2001**, *87*, 188102.